Voxel-by-voxel signal correlations between carbon-13 metabolic and perfusion agents in a rat breast cancer xenograft model by co-polarization of pyruvic acid and HP001

Justin Y.C. Lau[1,2], Albert P. Chen[3], Yiping Gu[2], William Dominguez-Viqueira[2], and Charles H. Cunningham[1,2]

[1]*Dept. of Medical Biophysics, University of Toronto, Toronto, Ontario, Canada,* [2]*Imaging Research, Sunnybrook Health Sciences Centre, Toronto, Ontario, Canada,* [3]*GE Healthcare, Toronto, Ontario, Canada*

Target audience: hyperpolarized media, metabolic imaging

Purpose: A prerequisite for *in vivo* hyperpolarized ^{13}C MR metabolic monitoring is the adequate perfusion of the tissue of interest such that the injected substrate can be delivered within the lifetime of the signal enhancement, which can be greater than four orders of magnitude.[1] Previous studies[2-6] have investigated the use of hyperpolarized HP001 (*bis*-1,1-hydroxymethyl-[1-^{13}C]cyclopropane-d_8) as an intravenous agent for perfusion measurement. We demonstrate dynamic observation of metabolism and perfusion with interleaved imaging and spectroscopic acquisition using co-polarized pyruvic acid and HP001 in a breast cancer xenograft model in rats.

Methods: Co-polarization: Neat [1-^{13}C] pyruvic acid and [1,2-$^{13}C_2$] pyruvic acid (Isotec) were combined 9:1 v/v, doped with 15 mM OX63 radical (Oxford) and 1 mM Gd chelate (Prohance®, Bracco International). Neat HP001 (Isotec) was doped with 15 mM OX63 and 1 mM Gd chelate. The two mixtures were placed into the sample vial 2:1 v/v at room temperature and polarized at 3.35 T, 0.8 K, and 94.058 GHz using a SpinLab DNP Polarizer (GE Healthcare). Imaging: Subcutaneous xenografts of MDA-MB-231 human breast cancer cell line with MS1 mouse endothelial cell line were prepared in male RNU nude rats as previously described.[7] Rats were placed in a dual-tuned ^{1}H/^{13}C rat coil (GE Healthcare) and imaged at 3.0 T using a GE MR750 scanner. After injection of 2 mL of pre-polarized substrate over 12 s via tail vein catheter, a 3D flyback echo-planar trajectory (TR/TE = 56/11.6 ms) was run to obtain 64 × 8 × 6 cm^3 volumetric data with 5 mm isotropic spatial resolution. Interleaved 18.8 ms spectral-spatial pulses were applied to excite lactate, pyruvate C_1, and HP001 with nominal tip angles of 30°, 2.5°, and 10° respectively, resulting in net excitations of 80°, 9°, and 34° per volume every 5 s. Spectroscopic acquisitions (262 ms readout, 31.25 kHz BW) with 1.8 ms slice-selective 5° pulses over 1 cm of the kidneys were performed once per imaging volume.

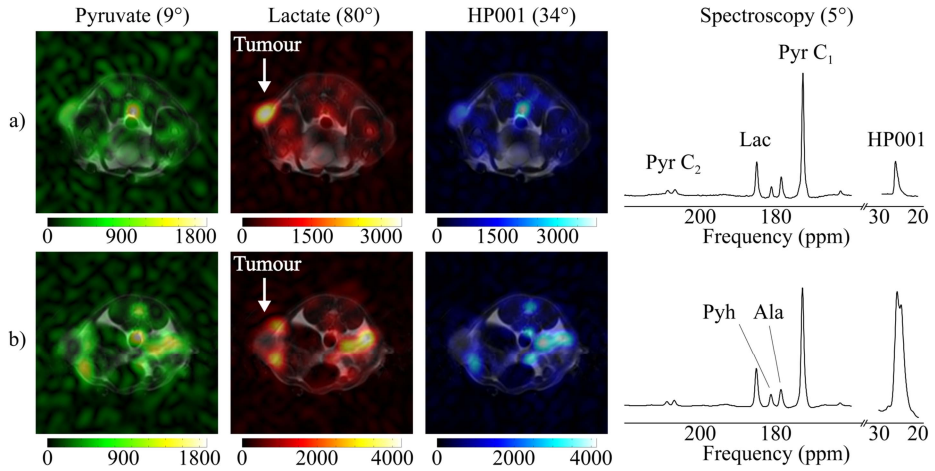

Figure 1: Overlay of anatomical and ^{13}C images of an axial slice through the tumour with corresponding spectra showing pyruvate (Pyr), lactate (Lac), pyruvate hydrate (Pyh), alanine (Ala), and HP001 resonances in a 1 cm slice centred over the kidneys for a) rat 2 (injection 1) and b) rat 5 (injection 1). Flip angles given represent the net excitation per volume. Spectroscopic acquisition facilitated off-resonance spatial shift correction based on EPI blip-reversal by providing reasonable initial frequency estimates.

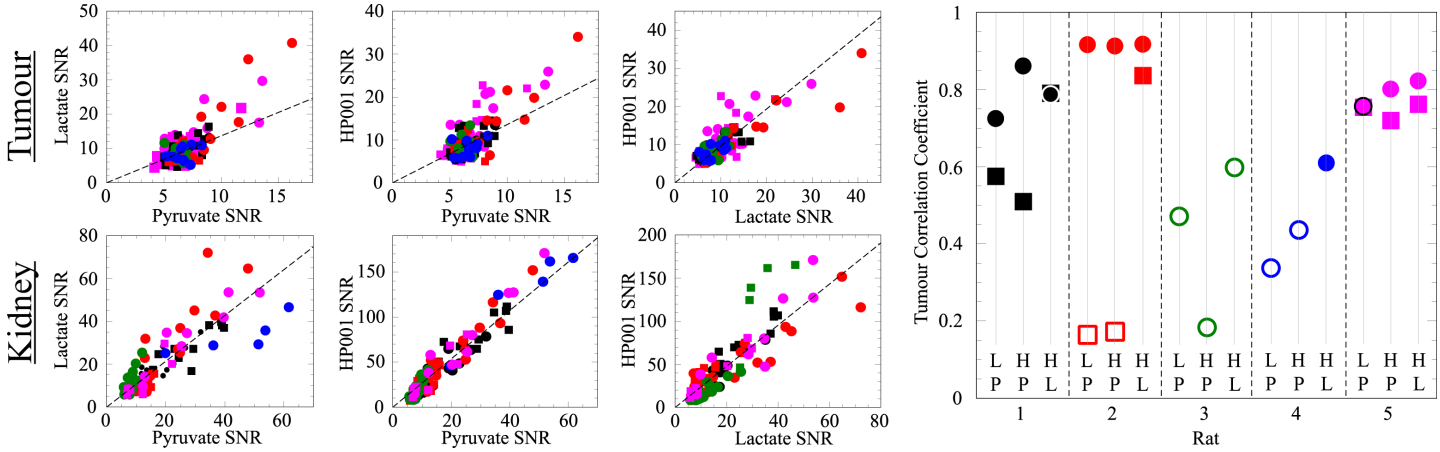

Figure 2: Voxel-by-voxel analysis of signal correlation in the tumour (top) and kidney (bottom). Each animal is denoted by a different colour. Repetitions on the same animal are denoted by different symbols. The dashed line represents the weighted linear regression of the combined data. The lactate-pyruvate (LP), HP001-pyruvate (HP), and HP001-lactate (HL) correlation coefficients are shown (right) for datasets of each animal with solid symbols representing statistical significance ($p < 0.05$).

Results: Axial images of the tumours for 2 of 5 animals included in this study, acquired approximately 30 s after the start of the injection, are shown in figure 1. Two repetitions (separate injections) were acquired for rats 1, 2, and 5. Frequencies for each agent were determined from the spectra and used as initial conditions for mutual information off-resonance spatial shift correction based on blip-reversal.[8] Anatomical images were used to manually segment pixels corresponding to the tumour and kidneys. For each voxel in the tumour or kidney, SNR was calculated by summing all time points (area under the curve) and displayed in figure 2 to show the signal relationship between pairs of metabolic/perfusion agents. In the kidney, there was a statistically significant correlation ($p < 0.05$) between pyruvate and HP001 for all 5 animals. A Pearson's correlation coefficient analysis (figure 2) suggests a stronger SNR correlation between lactate and HP001 than lactate and pyruvate in the tumour.

Discussion: In figure 1b, the heterogeneity in metabolism corresponded to reduced perfusion in the central tumour, suggesting the development of a necrotic core. Poor correlations with pyruvate in some animals may have resulted from poor perfusion in the tumour or low pyruvate SNR due to the smaller net flip angle. Normalization of lactate signal using the HP001 response may be reasonable if rapid metabolic conversion to lactate precludes observation of pyruvate signal or in cases where it would be desirable to minimize RF consumption of pyruvate polarization.

Conclusion: Co-polarization of pyruvic acid and HP001 provided complementary information that can distinguish between poor perfusion and lack of metabolism. A statistically significant ($p < 0.05$) correlation between pyruvate and HP001 SNR was observed in the rat kidney. For this breast cancer xenograft model, lactate SNR correlated with perfusion, but the correlation between lactate and HP001 was stronger than that between lactate and pyruvate.

Acknowledgements: The authors thank Jennifer Barry for veterinary care and the Natural Sciences and Engineering Research Council of Canada for funding support.

References: [1] J.H. Ardenkjær-Larsen *et al*. (2003) *PNAS* 100: 10158. [2] J. Wolber *et al*. (2004) *Nucl Instrum Meth A* 526: 173. [3] M.I. Kettunen *et al*. (2013) *MRM* 70(5): 1200. [4] C. von Morze *et al*. (2012) *Magn Reson Imaging* 30(3): 305. [5] C. von Morze *et al*. (2014) *MRM* 72(6): 1599. [6] N. Bahrami *et al*. (2014) *Quant Imaging Med Surg* 4(1): 24. [7] A.P. Chen *et al*. (2013) *PLOS ONE* 8(2): e56551. [8] W. Dominguez-Viqueira *et al*. (2012) *Proc ISMRM* 20: 4294.